Chaos, Solitons and Fractals 184 (2024) 114928

Contents lists available at ScienceDirect

Chaos, Solitons and Fractals

journal homepage: www.elsevier.com/locate/chaos

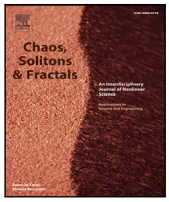

Coupling of neurons favors the bursting behavior and the predominance of the tripod gait

S. Serrano [a,*], R. Barrio [a], Á. Lozano [b], A. Mayora-Cebollero [a], R. Vigara [a]

[a] IUMA, CoDy and Dpto. Matemática Aplicada. Universidad de Zaragoza, E-50009 Zaragoza, Spain
[b] IUMA, CoDy and Dpto. Matemáticas. Universidad de Zaragoza, E-50009 Zaragoza, Spain

ARTICLE INFO

MSC:
37N25
37C27
92B20
92B25

Keywords:
Small networks
Insect movement
Tripod gait
Chaos
Hyperchaos
Bursting

ABSTRACT

In nature, it has been observed that the dominant locomotor pattern of hexapod insects is often the tripod gait. Our analysis of a Central Pattern Generator (CPG) of the insect movement gives reasons for this dominance: the mathematical CPG model presents the tripod pattern with bursting dynamics in a parametric region where an isolated neuron has a simpler behavior. That is, we show how the coupling of small networks of neurons makes the system to continue having bursting dynamics even when an isolated neuron would be spiking. Moreover, in parametric regions where a neuron shows chaotic dynamics, the CPG exhibits a chaotic synchronization phenomenon: the chaotic tripod gait. In other words, *coupling loves bursting... and tripod gait*. The hyperchaotic phenomenon is also present and we locate regions where up to four Lyapunov exponents are positive.

1. Introduction

In nature, insects mainly use the *tripod gait*, in which three legs move at a time while the other three remain stationary (see Fig. 1), to move quickly [1,2]. It has been shown in recent studies that mathematical models of patterns in networks [3,4] can help in the study of patterns in nature. Previous studies have shown that naturally occurring patterns in animals can be seen in Central Pattern Generators (CPGs), small groups of neurons able to generate rhythmic motor patterns even in absence of sensory input [5–8]. In robot design, a typical approach is using locomotion on wheels or tracks, but the use of legs in robots allows to operate on uneven terrain [9,10]. For this reason, there is a growing interest in using insect locomotion schemes to control walking robots. There are several models for insect locomotion based primarily on a six-neuron CPG (see [11–14]). Besides, robotics researchers [15–20] also use similar simplified models.

In this paper we consider a CPG with six coupled neurons following the model developed by Ghigliazza and Holmes [12]. In that work, the neural architecture of cockroach locomotion was described by the bursting model developed in [21] along with a single equation describing synaptic dynamics. On those articles a detailed analytical study is developed by assuming several simplification approaches, but those simplifications do not cover numerous non-symmetric patterns. Therefore, in [22,23] we presented a detailed numerical study combining different techniques, and we showed that the study of an isolated neuron not only provides a roadmap of the dynamics of that isolated neuron, but also for the coupled neurons of the CPG in a large parametric region. In [23] we also detailed the location of the different gait patterns in insect movement taking into account different parameters and how the system network can change until the insect reaches the dominant tripod gait.

But ... what happens in regions where the dynamics of the isolated neuron are not of the same type as the dynamics of the coupled neurons in the network? Is the tripod gait more ubiquitous than expected?

A key point to the study of different movement patterns is the maintenance of bursting behavior in the CPG. Bursting patterns [24,25] consist of alternating episodes of rapid spikes and intervals of quiescence or subthreshold oscillations. Bursting behavior is ubiquitous in the nervous system and is a key point in the generation of network rhythmic patterns [26]. The bursting neurons are of particular importance in rhythmically activate CPG networks, which control, for example, ongoing motor behaviors in locomotion [27]. Closely related to bursting behavior is the duty cycle, which is a crucial concept in neuroscience that describes the proportion of a cycle period in which

* Corresponding author.
E-mail addresses: sserrano@unizar.es (S. Serrano), rbarrio@unizar.es (R. Barrio), alozano@unizar.es (Á. Lozano), amayora@unizar.es (A. Mayora-Cebollero), rvigara@unizar.es (R. Vigara).

https://doi.org/10.1016/j.chaos.2024.114928
Received 19 December 2023; Received in revised form 25 March 2024; Accepted 22 April 2024
Available online 17 May 2024

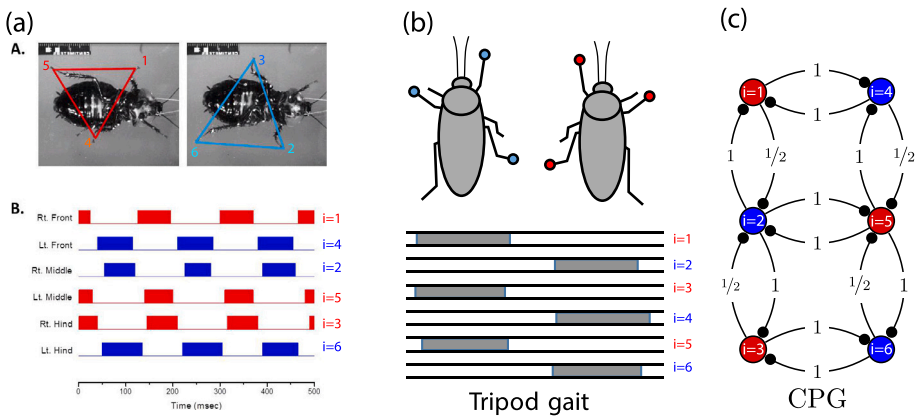

Fig. 1. (a) Experimental tripod gait pattern for a tethered cockroach (taken from Fig. 1 of [11]). (b) The schematic tripod gait. (c) The CPG used in the study. The solid bars in plots (a) and (b) indicate protraction (leg off ground and moving forward relative to the body and ground).

a neuron remains active. This concept is used to describe the activity of neurons and muscle fibers. When the number of spikes in a burst increases, so does the duty cycle, and therefore in bursting systems both studies (number of spikes and duty cycle) are very similar, and in this article we focus on studying the bursting dynamics. In nature, bursting activity can be generated by individual neurons (endogenous bursting) or by synaptic interactions within networks, as in a CPG. Note that network bursting does not require endogenous bursting [28]. Therefore, another related question is whether collective dynamics generate bursting dynamics in the CPG of insect movement when isolated neurons do not have endogenous bursting.

To answer these important questions, in this article we study in detail the parameter space out of the endogenous bursting region using different numerical techniques and obtaining the bifurcations of the main pattern routes detected in the parameter space using continuation techniques via the AUTO software [29,30]. Our study reveals the bifurcations that create and destroy the different routes and what is highly relevant, it shows how for large values of some parameters out of the endogenous bursting the tripod gait is also present and dominant [31]. Moreover, we have detected new phenomena in the CPG, like chaos, hyperchaos and chaotic synchronization (chaotic tripod gait).

This article is organized as follows. Section 2 introduces the equations of the CPG network. In Section 3 we present a study of the patterns experienced by the CPG model outside of the bursting area of isolated neurons. Section 4 is devoted to show how chaotic and hyperchaotic dynamics are present, while maintaining the tripod gait. Lastly, we present our conclusions at the end of the paper.

2. Insect movement CPG model equations

To solve the questions posed in the introduction we use the CPG model of the insect movement introduced in [12,32], which consists of a network of six mutually inhibiting identical neurons, each of which controls one leg of a cockroach. This model considers that inhibitory coupling is achieved via synapses that produce negative postsynaptic currents (I_{syn} in the equation below). Other considered currents are a fast nonlinear calcium current I_{Ca}, a slower potassium current I_K, an additional very slow current I_{KS}, a linear leakage current I_L and an external current I_{ext}. We only include nearest neighbor coupling and lateral symmetry. The complete model of the CPG (see Fig. 1(c) for the topology of the network and the values of the symmetric synapses) is described by an ODE system of dimension 24:

$$\begin{cases} C\dot{v}_i = -\Big[I_{Ca}(v_i) + I_K(v_i, m_i) + I_L(v_i) + I_{KS}(v_i, w_i)\Big] \\ \qquad + I_{\text{ext}} - (I_{\text{syn}})_i(v_i, s_j), \\ \dot{m}_i = \dfrac{\epsilon}{\tau_m(v_i)}[m_\infty(v_i) - m_i], \\ \dot{w}_i = \dfrac{\delta}{\tau_w(v_i)}[w_\infty(v_i) - w_i], \\ \dot{s}_i = \alpha s_\infty(v_i)(1 - s_i) - \beta s_i, \end{cases}$$

with $i = 1, 2, \ldots, 6$. Here, v_i are voltages, m_i and w_i are gating variables and s_i are the synapses variables. The different values of the extra current $(I_{\text{syn}})_i$ for each neuron potential v_i are:

$$\begin{aligned} (I_{\text{syn}})_1 &= c_1\, g_{\text{syn}}\, s_4(v_1 - E_s^{\text{post}}) + c_5\, g_{\text{syn}}\, s_2(v_1 - E_s^{\text{post}}), \\ (I_{\text{syn}})_2 &= c_2\, g_{\text{syn}}\, s_5(v_2 - E_s^{\text{post}}) + c_4\, g_{\text{syn}}\, s_1(v_2 - E_s^{\text{post}}) \\ &\quad + c_7\, g_{\text{syn}}\, s_3(v_2 - E_s^{\text{post}}), \\ (I_{\text{syn}})_3 &= c_3\, g_{\text{syn}}\, s_6(v_3 - E_s^{\text{post}}) + c_6\, g_{\text{syn}}\, s_2(v_3 - E_s^{\text{post}}), \\ (I_{\text{syn}})_4 &= c_1\, g_{\text{syn}}\, s_1(v_4 - E_s^{\text{post}}) + c_5\, g_{\text{syn}}\, s_5(v_4 - E_s^{\text{post}}), \\ (I_{\text{syn}})_5 &= c_2\, g_{\text{syn}}\, s_2(v_5 - E_s^{\text{post}}) + c_4\, g_{\text{syn}}\, s_4(v_5 - E_s^{\text{post}}) \\ &\quad + c_7\, g_{\text{syn}}\, s_6(v_5 - E_s^{\text{post}}), \\ (I_{\text{syn}})_6 &= c_3\, g_{\text{syn}}\, s_3(v_6 - E_s^{\text{post}}) + c_6\, g_{\text{syn}}\, s_5(v_6 - E_s^{\text{post}}). \end{aligned}$$

The parameter g_{syn} denotes synaptic strength, and we have considered a voltage based synapse model as in [12]. The auxiliary ionic current functions are defined by

$$I_{Ca}(v) = g_{Ca}\, n_\infty(v)\,(v - E_{Ca}), \qquad I_K(v) = g_K\, m\,(v - E_K),$$
$$I_L(v) = g_L\,(v - E_L), \qquad I_{KS}(v) = g_{KS}\, w\,(v - E_K),$$

and where the different time scales and steady state gating variables are

$$\tau_m(v) = \operatorname{sech}\big(k_{0_K}\,(v - V_K^{th})/2\big), \qquad \tau_w(v) = \operatorname{sech}\big(k_{0_{KS}}\,(v - V_{KS}^{th})/2\big),$$
$$m_\infty(v) = \big(1 + e^{-2k_{0_K}\,(v - V_K^{th})}\big)^{-1}, \qquad w_\infty(v) = \big(1 + e^{-2k_{0_{KS}}\,(v - V_{KS}^{th})}\big)^{-1},$$
$$n_\infty(v) = \big(1 + e^{-2k_{0_{Ca}}\,(v - V_{Ca}^{th})}\big)^{-1}.$$

The parameters C, ϵ and δ determine the time scales of v, m and w. If X denotes any of the considered ions, E_X is the Nernst potential, g_X is the maximal conductance, and k_{0_X} is the steepness of the transition happening at threshold potential V_X^{th}. See details on the parameters and the global dynamics in [12,22,23].

In the selection of the network parameters $\{c_i\}$ for the network (see Fig. 1(c)), we assume contralateral symmetry (between left and right side) and the input balance conditions

$$c_1 + c_5 = c_2 + c_4 + c_7 = c_3 + c_6, \qquad c_4 = c_7, \quad c_5 = c_6, \quad c_1 = c_3.$$

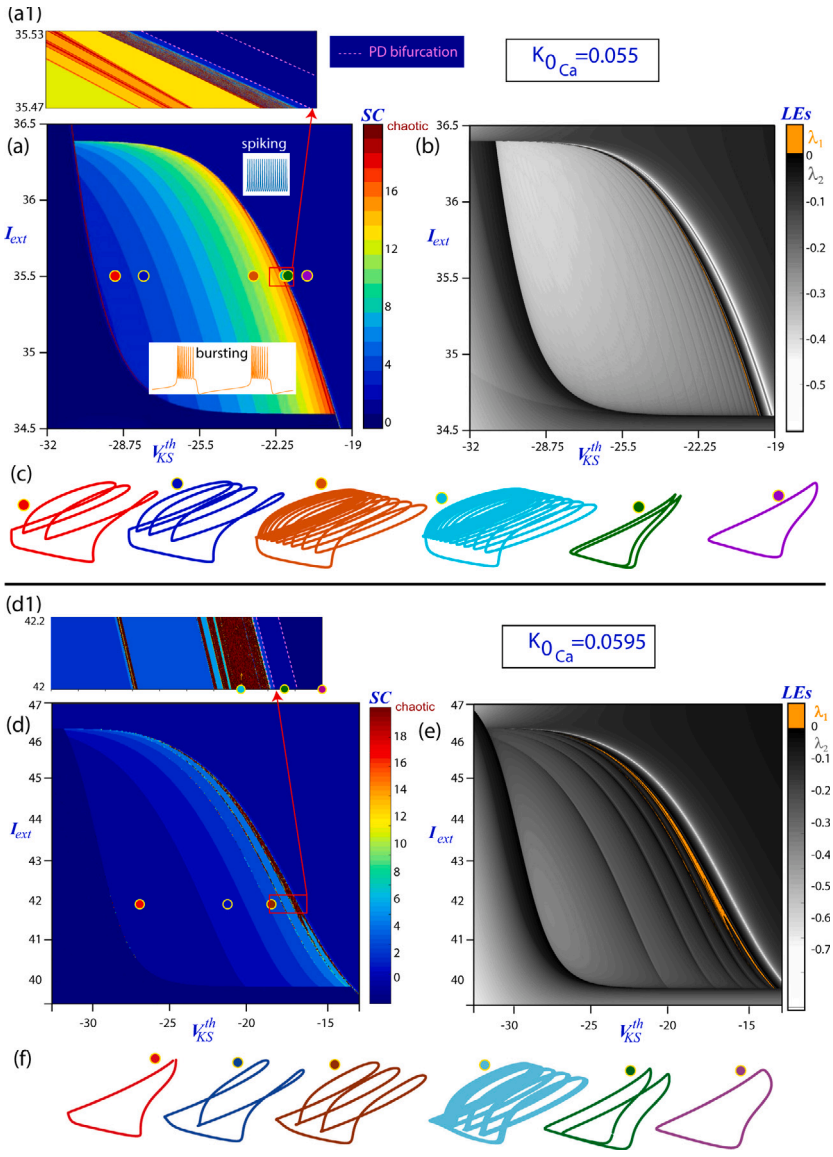

Fig. 2. Analysis of the bursting region of an isolated neuron using different techniques on the plane $(V_{KS}^{th}, I_{\text{ext}})$ for two values of the parameter $k_{0_{Ca}}$ (0.055 and 0.0595). (a) Spike-counting (SC) and (b) First and second Lyapunov exponents (λ_1 and λ_2, respectively) for $k_{0_{Ca}} = 0.055$. All of them provide similar information but with a different point of view. Small zoom on plot (a1) shows the narrow chaotic band and two period-doubling (PD) bifurcation curves. (c) Different stable periodic orbits (attractors). The parametric values are indicated by the corresponding color dots of panel (a). Some of the limit cycles show a period-doubling bifurcation (inside an infinite cascade) that finally leads to chaotic behavior. Plots (d), (d1), (e) and (f) present similar results but for $k_{0_{Ca}} = 0.0595$. (For interpretation of the references to color in this figure legend, the reader is referred to the web version of this article.)

So, by symmetry, we do not differentiate forward and backward movements in our tests. Moreover, we have set their values to

$$c_4 = c_7 = \frac{1}{2}, \qquad c_1 = c_2 = c_3 = c_5 = c_6 = 1.$$

2.1. Preliminary numerical study

In all the article, different sweeping techniques are used to show several uniparametric and biparametric analysis: the spike-counting, Lyapunov exponents and bifurcation analysis using continuation techniques.

The spike-counting technique [33] (also called isospike technique [34]) consists on selecting a Poincaré section or to impose a suitable condition (like to detect all the relative maxima of the orbit, what is the condition used in this article). And later, after a long transient integration to go to the asymptotic invariant, we use the selected condition to compute the corresponding points to detect the period and maxima (in our case) for the periodic case, or to put the maximum number of allowed points that means either chaotic behavior or a very long periodic orbit. In order to represent the different dynamics, a color is assigned to each number of maxima. To obtain the spike-counting plots we use the advanced capabilities of the Taylor series numerical integrator TIDES [35,36] that allows a continuous output, very suitable for the location of the maximum points of the orbits. The Runge–Kutta integrator of order 5 of Dormand–Prince [37] (with time step 0.001) is applied to obtain the time series that we need in the algorithm of Wolf et al. [38] to compute the Lyapunov exponents. The bifurcation analysis has been obtained with continuation techniques using the software AUTO [29,30].

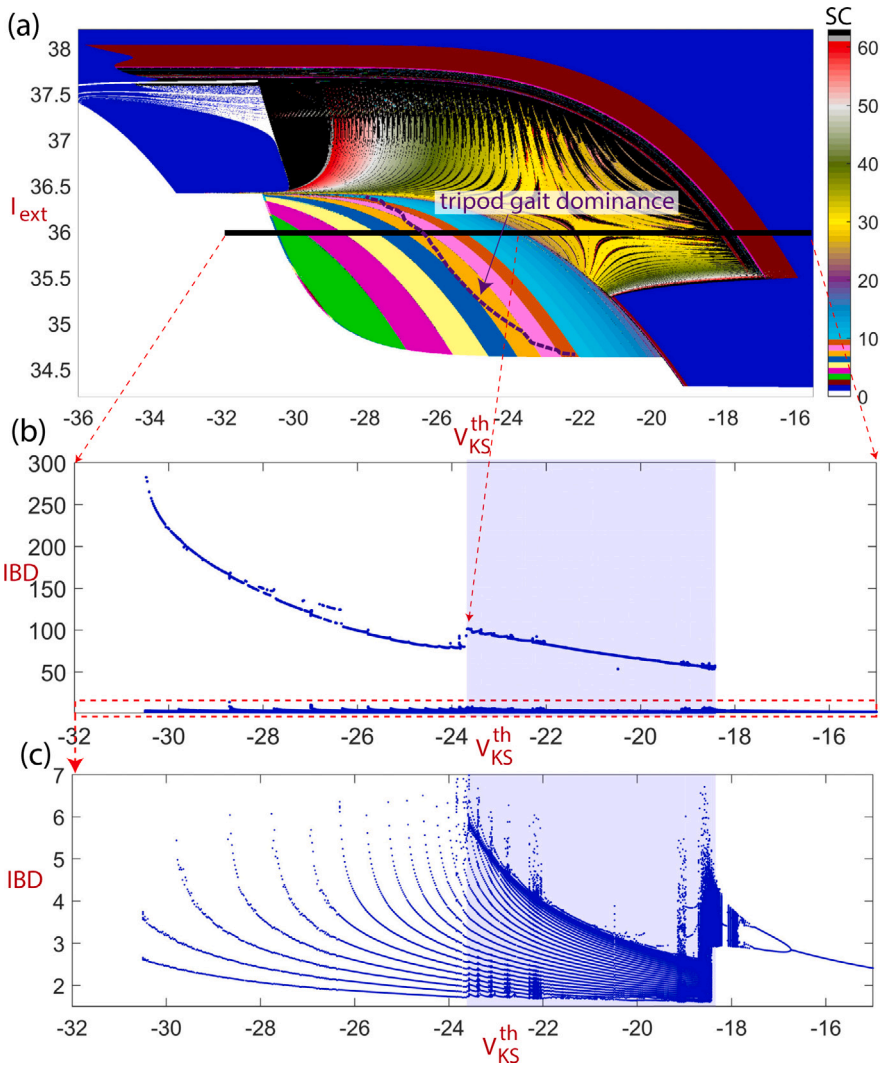

Fig. 3. Analysis of the complete CPG network. (a) Spike-counting of the plane $(V_{KS}^{th}, I_{\text{ext}})$ for $k_{0_{Ca}} = 0.055$ and $g_{\text{syn}} = 0.015$ showing the selected line $I_{\text{ext}} = 36$. (b) Interspike bifurcation diagram (IBD) on that line and (c) a magnification of the lower part of the IBD plot. (For interpretation of the references to color in this figure legend, the reader is referred to the web version of this article.)

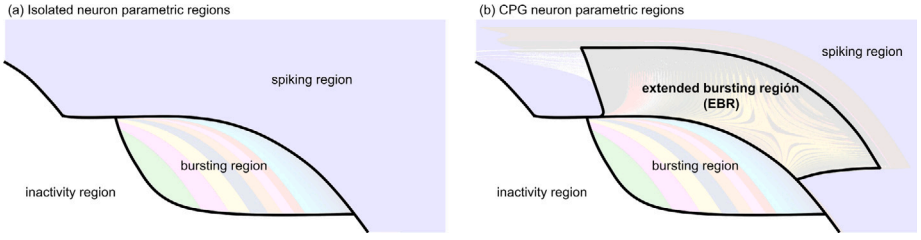

Fig. 4. Scheme of the different regions depending on the type of dynamics of (a) the isolated neuron and (b) the coupled neurons in the CPG. (For interpretation of the references to color in this figure legend, the reader is referred to the web version of this article.)

In the case of generic small networks we have recently proposed two numerical techniques to deal with small CPGs [22,23]. With those techniques we studied the different patterns of movement that appear in the insect CPG when the isolated neurons have endogenous bursting. Besides, in those articles we studied the different routes the CPG can follow to reach the dominant tripod gait. In this article we study what happens when the neurons in the network present a behavior different from that of neurons isolated for the same parametric values. In fact, the objective is to describe how the system network keeps the tripod gait with unexpected parameter values.

As mentioned above, the study of an isolated neuron allows the development of a roadmap to guide the changes in the different gaits and to know where to analyze the full model of the CPG. To make the study of an isolated motoneuron, we simply consider the first three variables

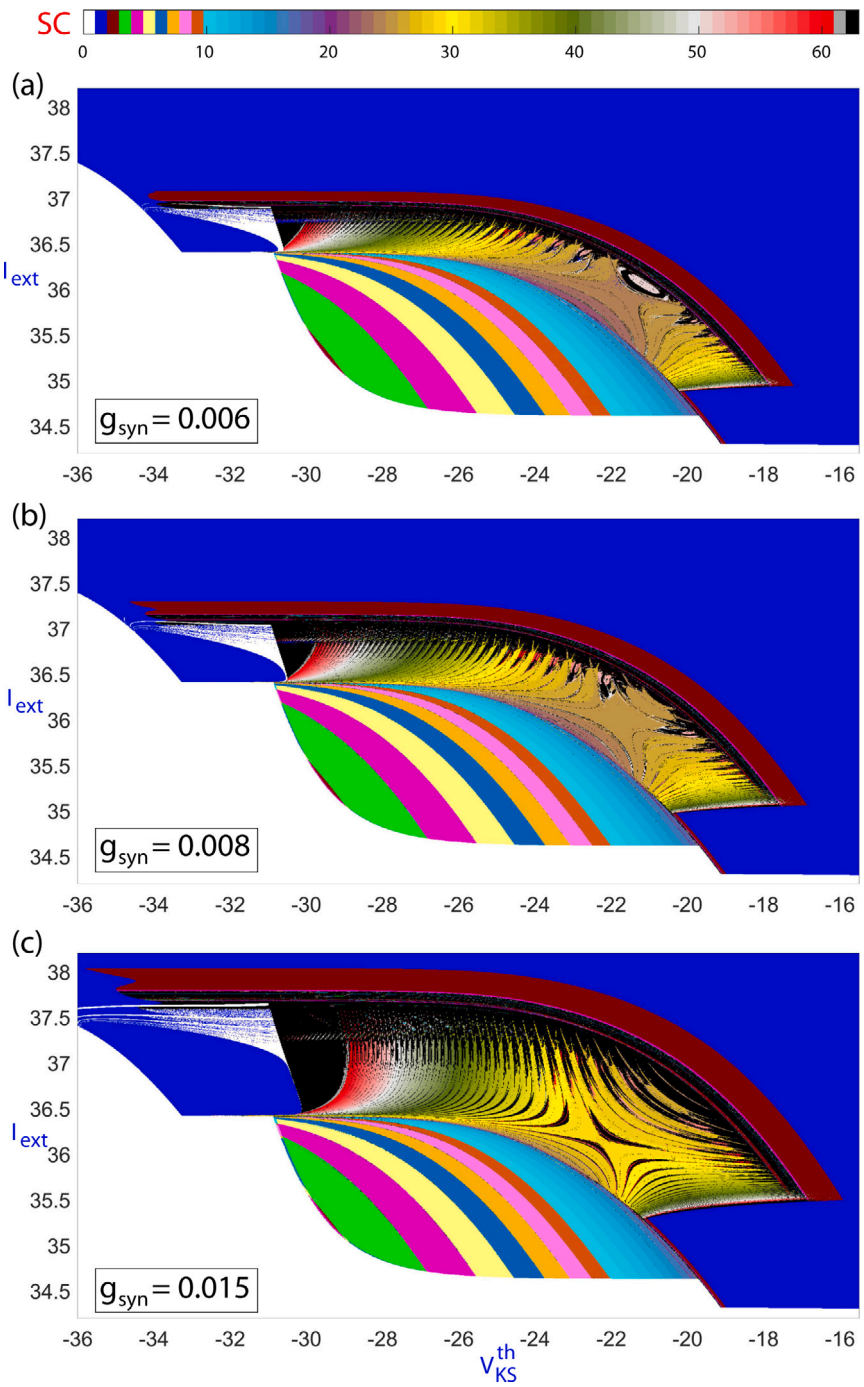

Fig. 5. Spike-counting of the plane $(V_{KS}^{th}, I_{\text{ext}})$ for $k_{0_{Ca}} = 0.055$ and for three values of $g_{\text{syn}} = 0.006$, 0.008 and 0.015. (For interpretation of the references to color in this figure legend, the reader is referred to the web version of this article.)

($i = 1$) and set $I_{\text{syn}} = 0$. In Fig. 2 we show the analysis of different sweeping techniques on the parameter plane $(V_{KS}^{th}, I_{\text{ext}})$ for two values of the parameter $k_{0_{Ca}}$, $k_{0_{Ca}} = 0.055$ and 0.0595 (V_{KS}^{th} is the threshold voltage considered in the expression of the derivative of the gating variable w and $k_{0_{Ca}}$ determines the extent of the transition region from the inactive to the active state, see [11] for more details). In plots (a) and (d) we use the spike-counting technique [39], where the color indicates the number of spikes per period of a periodic orbit. A large number (dark red) is associated with chaotic behavior. Specifically, the dark blue area (on the left side of the plot) represents the isolated neuron being inactive (equilibrium point). The slightly lighter blue area (right side) represents spiking behavior. The intermediate area (drop-shaped) with bands of different colors indicates bursting dynamics. Those bands mark the spike-adding process [40] where the bursting orbits add more spikes per orbit. In the latter zone, the CPG also shows bursting dynamics, and in the right part of it, about one third of the total area, corresponds to the tripod pattern in the CPG [23]. This process was studied in the insect moving framework [22,23], but what happens in a complete CPG model in the chaotic regions or outside the endogenous bursting area is an interesting open problem. The small insets (a1) and (d1) are zooms on the chaotic bands. Plots (b) and (e) present the first (when positive) and second (when the first is zero)

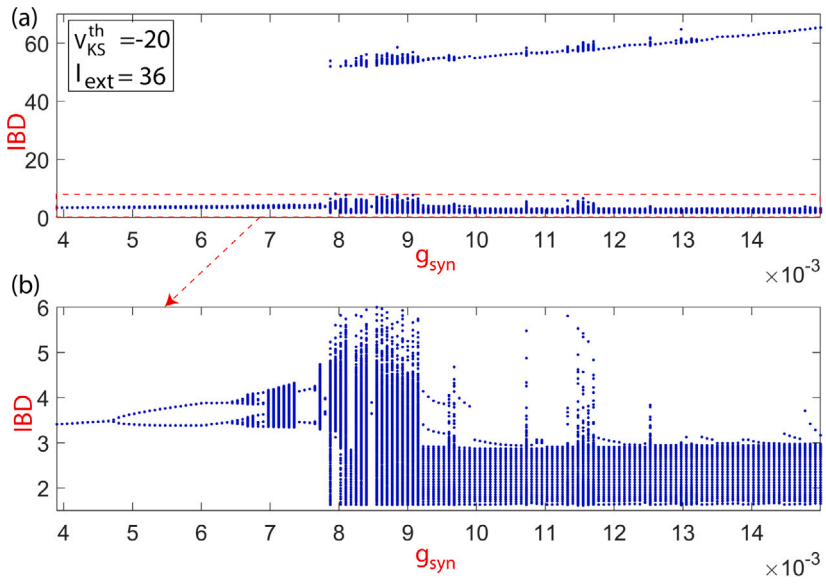

Fig. 6. (a) IBD results changing g_{syn} and fixing V_{KS}^{th} and I_{ext} (parametric point $(I_{ext}, V_{KS}^{th}) = (36, -20)$) in the region where isolated neuron experiences spiking behavior and (b) magnification of the lower part of the IBD diagram.

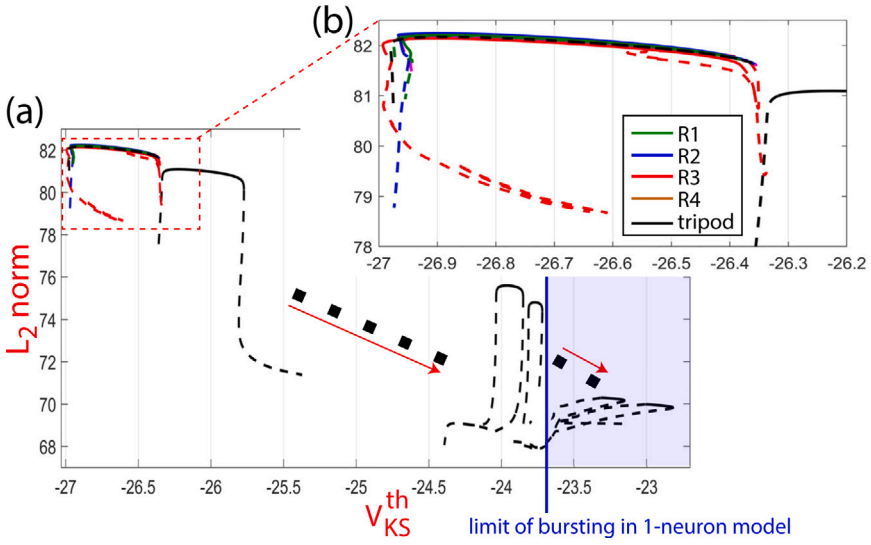

Fig. 7. (a) Families of periodic orbits (the gait movement patterns) obtained using continuation techniques (AUTO software) on the line $I_{ext} = 36$ (and $g_{syn} = 0.015$). (b) Magnification on the area where the different patterns of movement (R1, R2, R3 and R4) converge to the tripod gait [23].

Lyapunov exponents. We observe a total correspondence between both techniques. In the small plots (c) and (f) we show some selected orbits to illustrate different bursting (left) and spiking (right) behaviors. In both cases the light blue orbits are chaotic bursting.

3. Coupling and the bursting dynamics

As discussed in the introduction, in [23] we investigated what happens to the CPG dynamics when the parameters for the neurons are within the (drop-shaped) bursting region. We showed how, above a certain value of V_{KS}^{th} (which depends on I_{ext}), the CPG pattern is the tripod gait. The question we want to answer now is what happens in the coupled system (CPG) outside the bursting region.

Using the action potential of the first neuron, v_1, (similar results are obtained with the remaining neurons) we compute a spike-counting diagram for $g_{syn} = 0.015$, in an slightly larger parameter region that the one of Fig. 2(a). The result, in Fig. 3(a), shows the appearance of some structures on the right part outside the bursting area of a single neuron (compare with Fig. 2(a)). A natural question arises: What kind of dynamics do we have in this region?

In order to see with more detail the process on the "new" region, we have computed the interspike bifurcation diagram (IBD) on the marked line $I_{ext} = 36$. This diagram shows the time lags among consecutive spikes. Plot (b) shows the IBD diagram as described above, and (c) shows a zoom of the lower part of the IBD where the small interspike times are clustered (the large interspike values roughly corresponds to rest time of the neurons, i.e, the time among different bursts). In the right part of the studied interval we see that there is no upper branch of the IBD. This is due to the fact that this zone corresponds

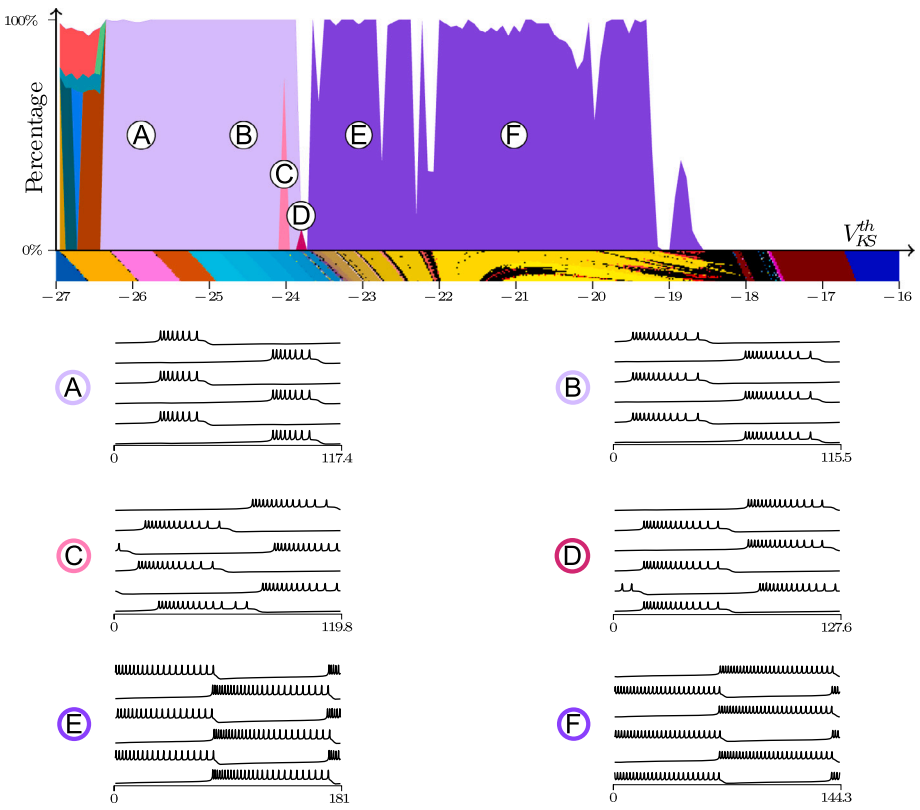

Fig. 8. The evolution of the tripod gait along the line $I_{\text{ext}} = 36$ and $g_{\text{syn}} = 0.015$. Each color represents a different pattern and how often it appears changing the initial conditions. Patterns (A) and (B) show the tripod pattern in the bursting region of an isolated neuron [22]. (C) and (D) are some noisy tripod-like patterns that appear just in the boundary of the bursting region of an isolated neuron. (E) and (F) are tripod patterns with overlapping in the EBR. (For interpretation of the references to color in this figure legend, the reader is referred to the web version of this article.)

to spiking dynamics. In the left part of the interval there are no points at all because the neurons are inactive (equilibrium point). On the other hand, in the rest of the interval, the dynamics are of the bursting type. That is, most of the newly detected region (in yellow and black in plot (a)) corresponds to bursting dynamics for the CPG. For this reason, we will call "extended bursting region" (EBR) to this region (see Fig. 4). On the left of the EBR, we observe the classical spike-adding process in the bursting dynamics. The blue shaded region in plots (b) and (c) is the area where the isolated neuron has spiking behavior, but the coupled neurons of the CPG burst. It can be seen how the spike-adding process continues. In addition, we observe small intervals where chaotic behavior appears to be occurring. In these small intervals, the structure defined by the lines marking each spike is broken. These intervals correspond to the intersection of the study segment ($I_{\text{ext}} = 36$) and the black stripes in the EBR shown in plot (a). We will return to these intervals in the next section.

Once it has been determined that the EBR is a bursting region for the CPG, we will analyze how the synchronization parameter (g_{syn}) affects it. Fig. 5 shows the result obtained with three different values of $g_{\text{syn}} = 0.006$, 0.008 and 0.015. We observe that the drop-shaped region where the isolated neuron undergoes bursting dynamics is not affected by the value of g_{syn}. The stronger the coupling, the larger the bursting region maintained by the CPG, as demonstrated by the colors of the new structures.

In order to study this evolution continuously, we chose the point $(I_{\text{ext}}, V_{KS}^{th}) = (36, -20)$ in the parameter plane and we compute the IBD for g_{syn} ranging from 0.004 to 0.015. Fig. 6(a) shows the results. Plot (b) gives a magnification of the lower part. We can see that the parametric point is initially in the region where the coupled neurons are spiking. As the value of g_{syn} increases, a usual period-doubling cascade leads to chaotic dynamics and then enters the region where the coupled neurons are bursting. The change in the behavior perfectly correlates with the increase in size of the EBR, and when the studied point crosses the boundaries of the different stripes (see Fig. 5).

In Fig. 6 we have shown that for a sufficiently large value of g_{syn} the coupled network maintains the bursting dynamics. That is ...*coupling loves bursting*. But, how are the families of bursting orbits organized in this region? Is there any new movement pattern? In [23], the authors studied the transition from different gaits of movement to tripod gait using bifurcation analysis. In Fig. 7 we briefly extend this bifurcation analysis to the EBR for $g_{\text{syn}} = 0.015$ on the line $I_{\text{ext}} = 36$. Using continuation techniques (AUTO software [29,30]), we compute different families of periodic orbits, that is, gait movement patterns. The first interval lasts until $V_{KS}^{th} \approx -26.4$ where different movement patterns (R1, R2, R3 and R4) become the tripod gait (see [23] for details). From that value onwards only the tripod gait is present. What is really interesting is that in the EBR we have tripod bursting families of periodic orbits as it is shown in the shadowed area of Fig. 7. On each family (on each curve) the number of spikes per burst is the same. Stable and unstable orbits are indicated with continuous and discontinuous lines on the plots, respectively. Each family has an upper tile where it is stable. This stable region of the family is the one detected by the spike-counting technique.

In [23] we designed a technique for studying the different patterns by means of an adapted Monte-Carlo scheme combined with a kind of machine-learning approach to classify the gaits. The *quasi Monte Carlo sweep* method (see [22] for a full description) consists of generating n different sets of initial conditions for each set of fixed parameter values. They are selected in a Halton sequence sampling that covers the range of each variable, i.e. $[-40, 10]$ for v_i and $[0, 1]$ for the remaining gating

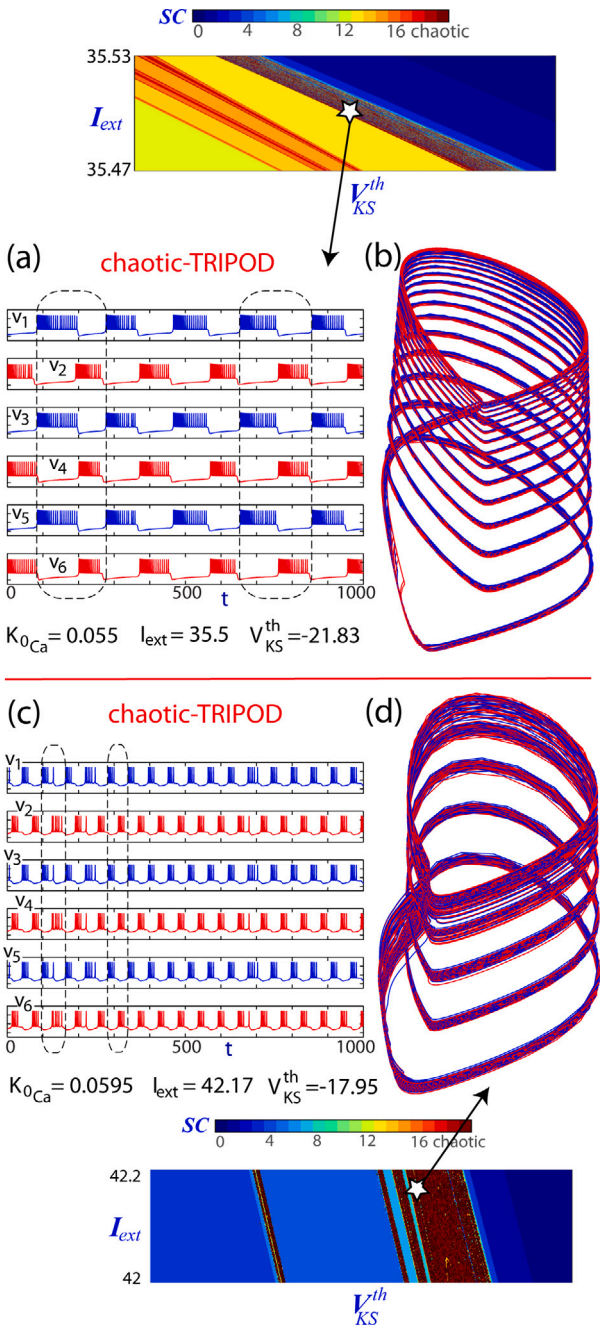

Fig. 9. (a) Synchronized chaotic tripod gait for $k_{0_{Ca}} = 0.055$ and (b) 3D plot of the evolution of the orbit showing a chaotic attractor. The small plot on the top shows the spike-counting of the plane (V_{KS}^{th}, I_{ext}) for $k_{0_{Ca}} = 0.055$ with a selected point (star) in the chaotic area. (c) Synchronized chaotic tripod gait for $k_{0_{Ca}} = 0.0595$. (d) A 3D view of the chaotic tripod gait. The small plot on the bottom shows the spike-counting of the plane (V_{KS}^{th}, I_{ext}) for $k_{0_{Ca}} = 0.0595$.

variables. This process is repeated for each neuron in the network. After a sufficiently large transient time, we begin to compute the pattern produced by the network and the state of the network at a given instant is stored. Subsequently, each sequence is analyzed using the Fast Fourier Transform to detect periodicity, storing them in a list. Finally, those patterns that represent the same signal must be detected to generate only one representative of its equivalence class. We can now estimate the "size" of the basin of attraction of each stable pattern as the fraction of the initial conditions that converge to it. This process has been carried out for a single set of parameters. By changing one of them, we can map the classes calculated for one parameter value to those of the other values, thus showing how the patterns evolve; for details, see [22].

Applying this technique on the line $I_{ext} = 36$ for $g_{syn} = 0.015$ we obtain the results shown in Fig. 8. On the top plot we have the percentage of the different gaits. On the left part there is a small segment with different gaits that give rise to different routes to tripod gait as explained in [23]. Later, the gait is always a tripod gait, but with some differences: At first, there is a time on the pattern with no active neuron (gaits –A– and –B–). After that, there are patterns (–C– and –D–) with some neurons where the length of the bursting is slightly different. These noisy patterns appear in the boundary of the bursting region of the isolated neuron. Subsequently there are patterns (–E– and –F–) where three neurons are active alternatively because the number of spikes has grown in such a way that there is no rest time for the CPG, but following always a tripod gait. This situation is analogous to what happens in quadrupeds when they gallop (all their legs are in the air at certain intervals) or in humans when they run. Then a region of chaotic dynamics appears, this situation will be studied in the next section. Finally, the dynamics of the network end up being spiking.

Note that these pictures provide a solid evidence on the persistence of the bursting tripod gait after the bursting dynamics have disappeared for an isolated neuron. This shows that the permanence of the bursting behavior allows the CPG to increase the area of the tripod pattern (which is larger the higher the coupling strength). That is, ... *coupling loves bursting ... and tripod gait.*

4. Chaos and high order hyperchaos in the extended bursting region

We commented in Section 2.1 that an isolated neuron may have chaotic dynamics. We also showed in the previous section that there are areas of the EBR where the neurons that make up the network have chaotic dynamics. In this section we will investigate how chaotic the dynamics of the CPG are in these areas.

In Fig. 9 we study two values of the parameters, shown in Fig. 2, exhibiting chaotic dynamics for an isolated neuron. Small inset above Fig. 9(a) presents the spike-counting diagram as in Fig. 2(a1), where the studied point has been highlighted with a star ($k_{0_{Ca}} = 0.055$, $V_{KS}^{th} = -21.83$ and $I_{ext} = 35.5$). As we can see, this point is inside the chaotic region of an isolated neuron. Fig. 9(b) shows the orbit of the 6 neurons in the network. The chaotic attractor is similar to a "fat" periodic orbit. The dynamics are also chaotic, like for an isolated neuron. However, if we look at plot (a), we can see the actual motion pattern produced by the CPG for this parameter selection and verify that in fact it is a *synchronized chaotic tripod gait.* Plots (c) and (d) present similar results but now in the chaotic area for $k_{0_{Ca}} = 0.0595$ of Fig. 2(d1). Note how the orbit of each neuron in the CPG exhibits chaotic behavior, just like the one of an isolated neuron would. However, the coupled CPG shows a clear tripod gait. That is, the system maintains a tripod gait independently of the dynamics of the bursting neurons once the tripod gait is the dominant pattern of movement. So, these are nice examples of chaotic synchronization phenomena caused by the coupling of the CPG.

To analyze what is happening in the EBR, we have computed the Lyapunov exponents on the line $I_{ext} = 36$. Fig. 10(a) is a zoom on the spike-counting diagram of the line given in Fig. 6, and plot (b) gives the first and second Lyapunov exponents. We observe that the Lyapunov exponents confirm the chaoticity on some regions, but they also evidence the existence of hyperchaotic dynamics since the second Lyapunov exponent is positive in some intervals. Note that recently the study of chaos and hyperchaos in different coupled systems has attracted numerous recent articles [41–44] using different techniques.

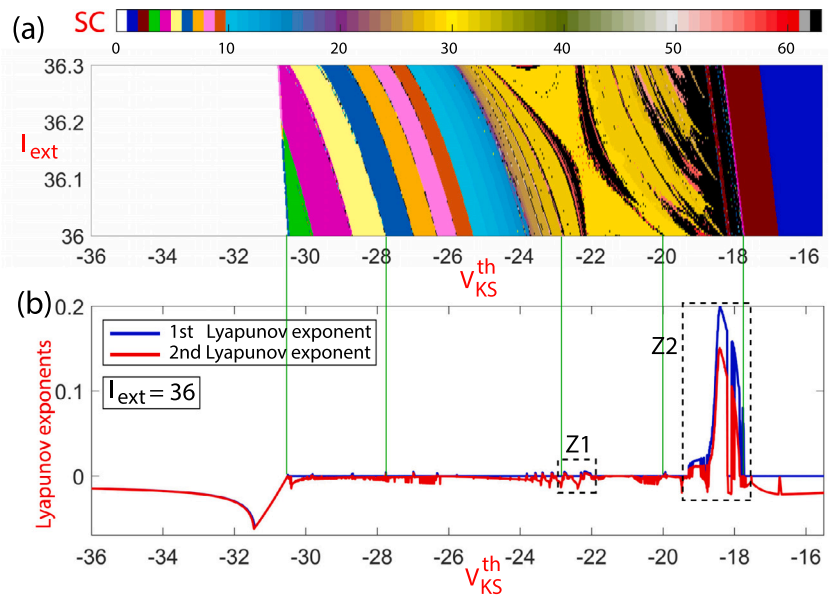

Fig. 10. (a) Spike-counting plot on a region with chaotic dynamics on the CPG. (b) First and second Lyapunov exponents on the line $I_{\text{ext}} = 36$ for $g_{\text{syn}} = 0.015$.

In Fig. 11 we explore the hyperchaos in the CPG. In the chaotic regions detected in Fig. 10 we have selected two segments, Z1 and Z2, in order to make a more detailed analysis. On plots (a1) and (a2) we show the spike-counting technique and the first and second Lyapunov exponents, respectively, on a small region around the line $I_{\text{ext}} = 36$ for $g_{\text{syn}} = 0.015$ on the segment Z1 of Fig. 10. We observe some areas where the second Lyapunov exponent is also positive, what means that we have hyperchaos (shaded regions). However, we can observe on plots (a3) and (a4), with $V_{KS}^{th} = -23.1$, that the behavior is similar to that already shown in Fig. 9: chaotic tripod. The reason seems to be the small magnitude of the positive exponents. On the other hand, if we look at the Z2 region (see plots (b1) and (b2)), we find up to four positive Lyapunov exponents, some with much higher values than those in Z1. In this case, if we look at the trajectory of the network and the patterns of the six neurons (for $V_{KS}^{th} = -18.6$, plots (b3) and (b4)), we see that there are intervals where the chaotic tripod continues to appear, but in other intervals there is only chaotic movement. We have seen how, as V_{KS}^{th} increases, the duration of the chaotic movement becomes longer and longer, until finally each neuron stops bursting and starts spiking. Therefore, it seems that the appearance of high-order hyperchaos breaks the chaotic synchronized tripod gait. It is also worth noting that there are not many examples of high-order hyperchaos in the literature for nature-inspired models.

Conclusions

In this article we have explored some differences between the dynamics of isolated neurons and connected ones in small networks. We have shown how the coupling of neurons in a small network (CPG) stabilizes the dynamics in the sense that the neurons maintain their dynamics over a larger parametric range than isolated neurons. In our case the system maintains bursting dynamics even when an isolated neuron would be spiking. It means that the network coupling facilitates bursting. Moreover, it favors the tripod gait, which is the main insect gait observed in nature. This fact is observed when the parameters of the model are selected in two different situations:

1. A single isolated neuron would be chaotic, coupled ones are chaotic one by one, but they are chaotically synchronized following a chaotic tripod gait;
2. A single isolated neuron would be spiking, the CPG produces a clean tripod gait, and its neurons one by one follow a bursting regime.

That is, *coupling loves bursting and tripod gait*.

Finally, we have detected hyperchaotic phenomenon (up to four positive Lyapunov exponents) in the chaotic synchronization region and we have seen that the appearance of this hyperchaotic phenomenon begins to break the synchronization. We leave for a future research a detailed study of the influence of hyperchaos in networks.

CRediT authorship contribution statement

S. Serrano: Writing – review & editing, Writing – original draft, Visualization, Validation, Conceptualization, Formal analysis, Investigation, Methodology, Software. **R. Barrio:** Investigation, Formal analysis, Conceptualization, Visualization, Writing – original draft, Writing – review & editing. **Á. Lozano:** Conceptualization, Investigation, Methodology, Software, Validation, Visualization, Writing – original draft, Writing – review & editing. **A. Mayora-Cebollero:** Investigation, Software, Validation, Visualization, Writing – original draft, Writing – review & editing. **R. Vigara:** Investigation, Software, Validation, Visualization, Writing – original draft, Writing – review & editing.

Declaration of competing interest

The authors declare that they have no known competing financial interests or personal relationships that could have appeared to influence the work reported in this paper.

Data availability

No data was used for the research described in the article.

Acknowledgments

RB, AL, AMC, SS and RV have been supported by the Spanish Research project PID2021-122961NB-I00. AL has been supported by the Spanish Research project PID2022-140556OB-I00 and by the European Regional Development Fund and Diputación General de Aragón (E22-23R). RB and SS have been supported by the Spanish Research project TED2021-130459B-I00 and by the European Regional Development Fund and Diputación General de Aragón (E24-20R, E24-23R and LMP94-21). SS has been supported by the Spanish Research project PID2019-105674RB-I00.

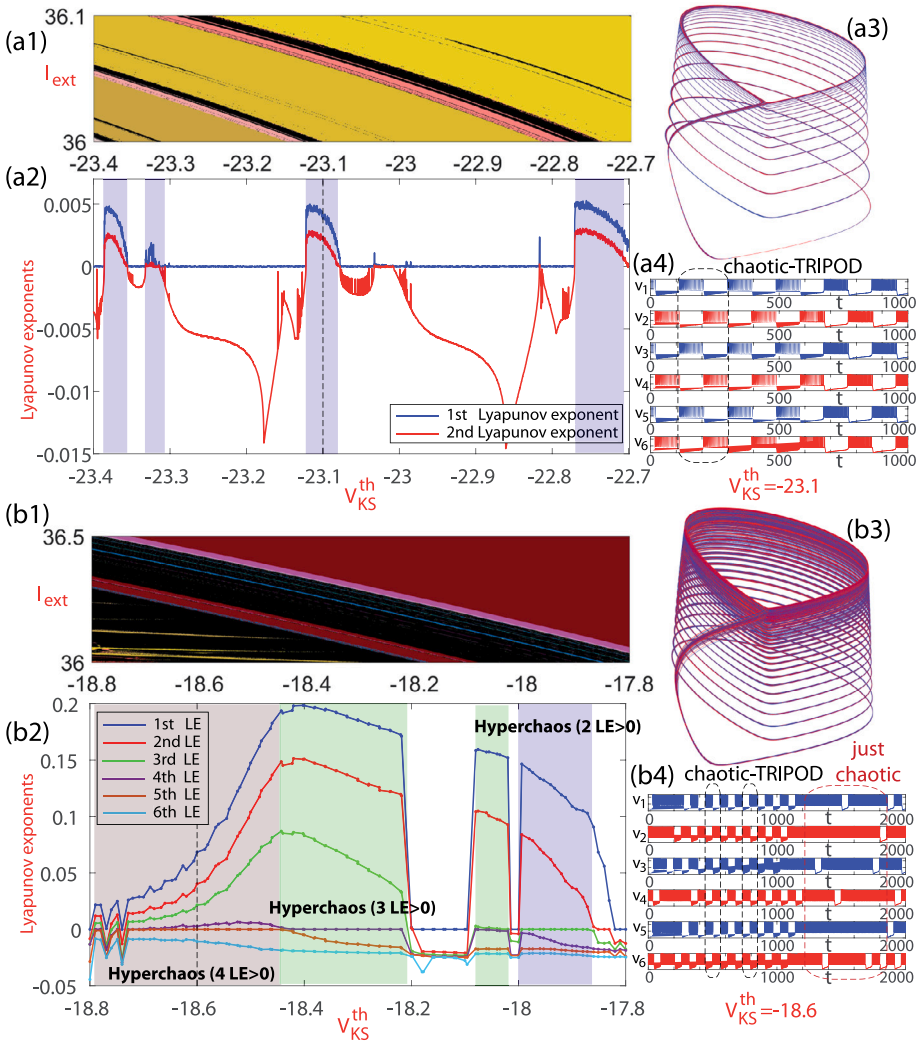

Fig. 11. (a1) Spike-counting on a small region around the line $I_{\text{ext}} = 36$ for $g_{\text{syn}} = 0.015$ on the segment Z1 of Fig. 10 and (a2) the first and second Lyapunov exponents (LE). Shaded areas correspond to hyperchaotic regions. (a3) 3D plot of the evolution of the orbit for $V_{KS}^{th} = -23.1$ and (a4) the corresponding synchronized chaotic tripod gait. (b1) and (b2) Spike-counting on the segment Z2 and the six first Lyapunov exponents, respectively. (b3) and (b4) the corresponding 3D plot of the orbit and gait patterns of voltage, respectively, for $V_{KS}^{th} = -18.6$.

References

[1] Chun C, Biswas T, Bhandawat V. *Drosophila* uses a tripod gait across all walking speeds, and the geometry of the tripod is important for speed control. eLife 2021;10:e65878.

[2] Ramdya P, Thandiackal R, Cherney R, Asselborn T, Benton R, Ijspeert AJ, Floreano D. Climbing favours the tripod gait over alternative faster insect gaits. Nature Commun 2017;8:14494.

[3] Ashwin P. Symmetric chaos in systems of three and four forced oscillators. Nonlinearity 1990;3(3):603–17.

[4] Rosenblum MG, Pikovsky AS, Kurths J. Phase synchronization in driven and coupled chaotic oscillators. IEEE Trans Circuits Syst I 1997;44(10):874–81.

[5] Marder E, Bucher D. Central pattern generators and the control of rhythmic movements. Curr Biol 2001;11(23):R986–96.

[6] Selverston A. Model neural networks and behavior. Berlin: Springer; 1985.

[7] Bal T, Nagy F, Moulins M. The pyloric central pattern generator in crustacea: a set of conditional neural oscillators. J Comp Physiol A 1996;163:715–27.

[8] Marder E, Calabrese R. Principles of rhythmic motor pattern generation. Physiol Rev 1996;76:687–717.

[9] Li C, Zhang T, Goldman DI. A terradynamics of legged locomotion on granular media. Science 2013;339(6126):1408–12. http://dx.doi.org/10.1126/science.1229163.

[10] Chong B, He J, Soto D, Wang T, Irvine D, Blekherman G, Goldman DI. Multilegged matter transport: A framework for locomotion on noisy landscapes. Science 2023;380(6644):509–15. http://dx.doi.org/10.1126/science.ade4985.

[11] Ritzmann R, Zill SN. Neuroethology of insect walking. Scholarpedia 2013;8(9):30879.

[12] Ghigliazza R, Holmes P. A minimal model of a central pattern generator and motoneurons for insect locomotion. SIAM J Appl Dyn Syst 2004;3(4):671–700.

[13] Ayali A, Borgmann A, Büschges A, Couzin-Fuchs E, Daun-Gruhn S, Holmes P. The comparative investigation of the stick insect and cockroach models in the study of insect locomotion. Curr Opin Insect Sci 2015;12:1–10.

[14] Fujiki S, Aoi S, Funato T, Tomita N, Senda K, Tsuchiya K. Hysteresis in the metachronal-tripod gait transition of insects: A modeling study. Phys Rev E 2013;88:012717.

[15] Campos R, Matos V, Santos C. Hexapod locomotion: A nonlinear dynamical systems approach. In: IECON 2010 - 36th annual conference on IEEE industrial electronics society. 2010, p. 1546–51.

[16] Tedeschi F, Carbone G. Design issues for hexapod walking robots. Robotics 2014;3(2):181–206.

[17] Ferrell C. A comparison of three insect-inspired locomotion controllers. Robot Auton Syst 1995;16(2):135–59.

[18] Spagna JC, Goldman DI, Lin P-C, Koditschek DE, Full RJ. Distributed mechanical feedback in arthropods and robots simplifies control of rapid running on challenging terrain. Bioinspiration Biomim 2007;2(1):9–18.

[19] Collins JJ, Stewart I. Hexapodal gaits and coupled nonlinear oscillator models. Biol Cybernet 1993;68(4):287–98.

[20] Herrero-Carrón F, Rodríguez FB, Varona P. Bio-inspired design strategies for central pattern generator control in modular robotics. Bioinspiration Biomim 2011;6(1):016006.

[21] Ghigliazza R, Holmes P. Minimal models of bursting neurons: How multiple currents, conductances, and timescales affect bifurcation diagrams. SIAM J Appl Dyn Syst 2004;3(4):636–70.
[22] Barrio R, Lozano Á, Rodríguez M, Serrano S. Numerical detection of patterns in CPGs: Gait patterns in insect movement. Commun Nonlinear Sci Numer Simul 2020;82:105047.
[23] Barrio R, Lozano Á, Martínez M, Rodríguez M, Serrano S. Routes to tripod gait movement in hexapods. Neurocomputing 2021;461:679–95.
[24] Izhikevich EM. Neural excitability, spiking and bursting. Int J Bifurcation Chaos 2000;10(06):1171–266.
[25] Fox DM, Rotstein HG, Nadim F. Bursting in neurons and small networks. In: Jaeger D, Jung R, editors. Encyclopedia of computational neuroscience. New York, NY: Springer New York; 2013, p. 1–17.
[26] Nusbaum M, Beenhakker M. A small-systems approach to motor pattern generation. Nature 2002;417:343–50.
[27] Marder E, Bucher D, Schulz D, Taylor A. Invertebrate central pattern generation moves along. Curr Biol 2005;15:R685–99.
[28] Selverston A, Szucs A, Huerta R, Pinto R, Reyes M. Neural mechanisms underlying the generation of the lobster gastric mill motor pattern. Front Neural Circuits 2009;3.
[29] Doedel E. AUTO: a program for the automatic bifurcation analysis of autonomous systems. Congr Numer 1981;30:265–84.
[30] Doedel EJ, Paffenroth R, Champneys AR, Fairgrieve TF, Kuznetsov YA, Oldeman BE, Sandstede B, Wang XJ. AUTO2000, http://cmvl.cs.concordia.ca/auto.
[31] Reches E, Knebel D, Rillich J, Ayali A, Barzel B. The metastability of the double-tripod gait in locust locomotion. iScience 2019;12:53–65.
[32] Aminzare Z, Srivastava V, Holmes P. Gait transitions in a phase oscillator model of an insect central pattern generator. SIAM J Appl Dyn Syst 2018;17(1):626–71.
[33] Barrio R, Shilnikov A. Parameter-sweeping techniques for temporal dynamics of neuronal systems: case study of Hindmarsh-Rose model. J Math Neurosci 2011;1(1):1–22.
[34] Freire JG, Gallas JAC. Stern–Brocot trees in the periodicity of mixed-mode oscillations. Phys Chem Chem Phys 2011;13:12191–8.
[35] Abad A, Barrio R, Blesa F, Rodríguez M. TIDES: a Taylor Integrator for Differential EquationS. ACM Trans Math Softw 2012;39:5:1–28.
[36] Abad A, Barrio R, Blesa F, Rodríguez M. TIDES web page. 2011, http://gme.unizar.es/software/tides.
[37] Hairer E, Nørsett SP, Wanner G. Solving ordinary differential equations I: Nonstiff problems. Berlin, New York: Springer-Verlag; 1993.
[38] Wolf A, Swift JB, Swinney HL, Vastano JA. Determining Lyapunov exponents from a time series. Phys D 1985;16(3):285–317.
[39] Barrio R, Shilnikov A. Parameter-sweeping techniques for temporal dynamics of neuronal systems: case study of Hindmarsh-Rose model. J Math Neurosci 2011;1:6:1–22.
[40] Barrio R, Ibáñez S, Pérez L, Serrano S. Spike-adding structure in fold/hom bursters. Commun Nonlinear Sci Numer Simul 2020;83:105100.
[41] Lin H, Wang C, Yu F, Hong Q, Xu C, Sun Y. A triple-memristor hopfield neural network with space multistructure attractors and space initial-offset behaviors. IEEE Trans Comput-Aided Des Integr Circuits Syst 2023;42(12):4948–58.
[42] Deng Q, Wang C, Lin H. Memristive Hopfield neural network dynamics with heterogeneous activation functions and its application. Chaos Solitons Fractals 2024;178:114387.
[43] Leo Kingston S, Kapitaniak T, Dana SK. Transition to hyperchaos: Sudden expansion of attractor and intermittent large-amplitude events in dynamical systems. Chaos 2022;32(8):081106.
[44] Stankevich N, Bobrovskii A, Shchegoleva N. Chaos and hyperchaos in two coupled identical Hindmarsh – Rose systems. Regul Chaotic Dyn 2024;29:120–33.